Journal of Materials Chemistry A

Accepted Manuscript

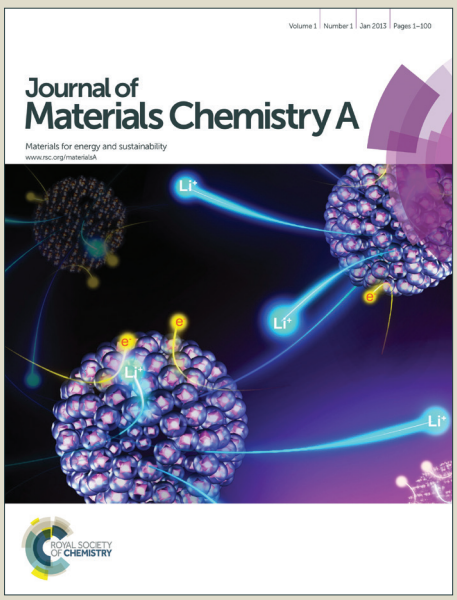

ROYAL SOCIETY OF CHEMISTRY

www.rsc.org/materialsA

Journal Name

RSCPublishing

ARTICLE

Electrospun Cr-doped $Bi_4Ti_3O_{12}/Bi_2Ti_2O_7$ Heterostructures Fibers with Enhanced Visible-Light Photocatalytic Properties

Cite this: DOI: 10.1039/x0xx00000x

Received 00th January 2012,
Accepted 00th January 2012

DOI: 10.1039/x0xx00000x

www.rsc.org/

Hongfei Shi,[ab] Huaqiao Tan,[ab]* Wan-bin Zhu, [c] Zaicheng Sun,[a]* Yuejia Ma [a] and Enbo Wang[b]*

A series of Cr-doped $Bi_4Ti_3O_{12}/Bi_2Ti_2O_7$ (BTO) heterostructures fibers have been synthesized by one-step of facile and economical electrospinning/calcination route. SEM and TEM results reveal that the diameters of the as-prepared fibers are 100 ± 30 nm in size. The light adsorption of $Bi_4Ti_3O_{12}$ and $Bi_2Ti_2O_7$ in the fibers has been improved remarkable by Cr doped. And with increasing the content of Cr doping, XRD and XPS shows that the amount of $Bi_2Ti_2O_7$ increases in the fibers. As a result, the $Bi_4Ti_3O_{12}/Bi_2Ti_2O_7$ heterojunction structure has been enhanced, which further promote the charge separation of photogenerated charge carriers. Photocatalytic tests display that the as-prepared Cr-doped $Bi_4Ti_3O_{12}/Bi_2Ti_2O_7$ fibers exhibit good photocatalytic activity for photodegradation of methyl orange (MO) under visible light irradiation.

Introduction

Recently, with the increasing serious of environmental deterioration and energy crisis, much effort has been paid to exploit new semiconductor catalysts with high photocatalytic properties for environmental applications,[1-4] water splitting,[5,6] and CO_2 conversion.[7-10] Bi-based semiconductors such as BiOX (X = Cl, Br, I),[11] $BiVO_4$,[12] Bi_2WO_6,[13] Bi_2MoO_6,[14] Bi_2O_3,[15] Bi_2S_3[16] and bismuth titanate,[17] as a new kind of promising candidates for visible light-driven catalysts have attracted considerable interest because of its high photocatalytic performances.[18] Bismuth titanate is a large Bi-Ti-O family, which includes several phases such as $Bi_{20}TiO_{32}$, $Bi_{12}TiO_{20}$, $Bi_2Ti_2O_7$, $Bi_4Ti_3O_{12}$ and $Bi_2Ti_4O_{11}$.[19] In the family, $Bi_{20}TiO_{32}$,[20] $Bi_{12}TiO_{20}$[21] and $Bi_2Ti_2O_7$[22] have been demonstrated as an effective visible light photocatalyst. Among these compounds, $Bi_4Ti_3O_{12}$ is a layered perovskite compound, which is constructed by the alternative stacking of $(Bi_2O_2)^{2+}$ layers and perovskite-like $(Bi_2Ti_3O_{10})^{2-}$ layers along the c axis.[23,24] Since Kudo and co-workers reported $Bi_4Ti_3O_{12}$ photocatalytic activity for water splitting,[25] $Bi_4Ti_3O_{12}$ has received much attention. $Bi_4Ti_3O_{12}$ was usually synthesized by a solid-state reaction or a decomposition method. But both of the two approaches have a limit to synthesize its nanostructural morphology with high surface areas and crystallinity. Therefore, a more simple and rational method to obtain the nanostructured $Bi_4Ti_3O_{12}$ is highly demanded.[26]

It is well known that electrospinning is one of the most convenient, universal and effective way to prepare nanostructural compounds with various morphologies.[27,28] Very recently, Hu et al. have demonstrated that electrospinning is a facile and effective method to synthesize 1D porous $Bi_4Ti_3O_{12}$ fibers.[29,30] But these synthesized $Bi_4Ti_3O_{12}$ fibers show a relative low visible light photocatalytic activity because of its intrinsic properties such as wide band gap (3.0 eV) and low capability for the separation of photogenerated charge carriers. To date, although many excellent works have been devoted to enhance the photocatalytic effciency of $Bi_4Ti_3O_{12}$ under visible light irradiation such as doping with metals[31-33] and combining with another narrow band gap semiconductor,[34-36] the development of high efficiency visible-light-driven $Bi_4Ti_3O_{12}$ photocatalyst are still highly desired.

Herein, we have fabricated a series of Cr-doped $Bi_4Ti_3O_{12}/Bi_2Ti_2O_7$ (BTO) heterostructures fibers by one-step of facile and economical electrospinning/calcination route. The diameters of the nanofibers are 70-130 nm in size. The band gaps of $Bi_4Ti_3O_{12}$ and $Bi_2Ti_2O_7$ have been narrowed due to the doping of Cr, resulting in the spectral absorption of fibers in visible light has been significantly improved. In addition, with the increasing of Cr doping, the amount of Bi_2TiO_7 increases in the electrospun fibers. As a result, the $Bi_4Ti_3O_{12}/Bi_2Ti_2O_7$ heterojunction structure has been enhanced, which further promote the charge separation of photogenerated charge carriers. Thus, the as-prepared photocatalysts exhibit a remarkable enhanced visible-light photocatalytic activity for

degradation of methyl orange (MO) than that of the initial $Bi_4Ti_3O_{12}/Bi_2Ti_2O_7$.

Expermental

Chemicals and materials

$Bi(NO_3)_3\ 5H_2O$, $Cr(NO_3)_3\ 9H_2O$, tetrabutyl titanate (TBT), ethanol (CH_3CH_2OH), and N,N-dimethylformamide (DMF) were purchased from Aladdin Chemical Co., Ltd., China. Poly(vinylpyrrolidone) (PVP, MW≈1,300,000) was obtained from Alfa Aeser. And all the chemicals were used without further purification.

Preparation of Cr-doped $Bi_4Ti_3O_{12}/Bi_2Ti_2O_7$ fibers

1.0 g of PVP was dissolved in 15 mL DMF/ethanol (volume ratio, 1: 1) mixture solution. After stirring for 60 minutes, 2 mL glacial acetic acid, 0.97 g (2 mmol) of $Bi(NO_3)_3\ 5H_2O$, 0.51 g (1.5 mmol) of TBT, $Cr(NO_3)_3\ 9H_2O$ (0.01g, 0.02g, 0.04g, 0.06 and 0.08 g, respectively) were added into the solution. And then the mixture of PVP-$Bi(NO_3)_3\ 5H_2O$-TBT-$Cr(NO_3)_3\ 9H_2O$ was stirred till to form clear solution. The above solution was loaded into a 10 mL plastic syringe connected with a 22 gauges blunt needle. The solution feed-rate was set at 0.5 mL h^{-1} controlled by a syringe pump. The metallic needle clamped with an electrode was connected to a variable high-voltage power supply, and a collector of an aluminum foil was used as a grounded counter electrode 15 cm away from the tip of the needle. The PVP - $Bi(NO_3)_3\ 5H_2O$ - TBT-$Cr(NO_3)_3\ 9H_2O$ composite fibers were formed at a high voltage of 15 kV. The electrospun precursor fibers were calcined at 600 ^oC with a heating rate of 2 $^oC\ min^{-1}$ in air for 1h. By this method, The Cr-doped $Bi_4Ti_3O_{12}/Bi_2Ti_2O_7$ (BTO) nanofibers with different Cr contents (the amount of $Cr(NO_3)_3\ 9H_2O$: 0.01 g, 0.02 g, 0.04 g, 0.06 g and 0.08 g, respectively) have been fabricated and denoted as BTO-0.01, BTO-0.02, BTO-0.04, BTO-0.06 and BTO-0.08, respectively.

Characterization

The UV-Vis absorption spectra were collected on a UV-2600 UV-Vis spectrophotometer (Shimadzu), with an integrating sphere, and $BaSO_4$ was used as the reference. X-Ray diffraction (XRD) analysis was recorded on a Bruker AXS D8 Focus using filtered Cu Ka radiation (λ= 1.54056 Å). A JEOL JSM 4800F SEM coupled with an energy-dispersive X-ray (EDX) spectrometer was used to characterize the morphology of the samples. TEM (transmission electron microscopy) and high-resolution TEM images were measured on an FEI Tecnai G2 operated at 200 kV. XPS were carried out on an ESCALABMKII spectrometer with an Al-Kα (1486.6 eV) achromatic X-ray source. The PL spectra were recorded on a Hitachi F-7000 spectrophotometer. The excitation wavelength is 320 nm.

Photocatalytic degradation of methyl orange

The photocatalytic activities of the as-prepared samples were evaluated by the degradation of methyl orange (MO) solution using a 300 W Xe lamp with a 420 nm cut-off filter as light source and a self-made glass vessel with a water-cooling jacket as reactor. The irradiation distance between the lamp and the mixture solution was 15 cm. 40 mg of photocatalyst was dispersed in 40 mL 20 ppm of MO solution (pH = 1). Before irradiation, the solution was stirred in the dark for 60 min to assure the adsorption-desorption equilibrium between the organic molecules and the catalyst surface was reached. After irradiation for a designated time, 1.5 mL of the reaction solution was taken, centrifuged, and measured on a Shimadzu UV-vis spectrometer UV-2600 at a maximum absorption wavelength of 506 nm.

Photoelectrode preparation

According to the procedure in references,[37, 38] electrophoretic deposition was used to deposited $Bi_4Ti_3O_{12}/Bi_2Ti_2O_7$ and BTO-0.08 on a FTO glass substrate, respectively. As shown in following: 40 mg of as-prepared sample was dispersed in a 50 mL of 0.2 mg/mL I_2/acetone solution under ultrasonic treatment. A two-electrode process was used to deposit the samples at 25 V for 15 min. Both electrodes were FTO glass substrates with the coated area about 1 × 4 cm^2. And then the deposited electrode was dried at 200 ^oC for 30 min to remove I_2 residues.

Photoelectrochemical measurements

The photoelectrochemical measurements of samples were investigated by a conventional three-electrode process in a quartz cell. A deposited BTO FTO photoanode, Pt foil and Hg/Hg_2Cl_2 electrode served as the working electrode, counter electrode and reference electrode, respectively. A 0.5 M Na_2SO_4 aqueous solution was used as the electrolyte. The photoanode was illuminated by a Beijing Trusttech Co. Ltd, PLS-SXE-S500 300 W Xe lamp. The illuminated area was about 1×1 cm^2.

Results and discussion

Structure Features and Physical Properties

The morphology and microstructure of the as prepared $Bi_4Ti_3O_{12}/Bi_2Ti_2O_7$ and BTO-0.08 fibers was shown in Fig. 1. It can be clearly seen from the SEM images that these fibers before calcination possess a relative smooth and uniform surface. The average diameters of the fibers were about 150 ± 30 nm, and its length was as long as several millimeters. After annealed at 600 ^oC, the fibrous morphology of $Bi_4Ti_3O_{12}/Bi_2Ti_2O_7$ and BTO-0.08 fibers is well maintained. As shown in Fig.1b and 1d, the diameters of the fibers were reduced to 100±30 nm. And these fibers become coarse and porous. Transmission electron microscopy (TEM) images further provide the detailed microstructure of BTO-0.08. As shown in Fig. 1e, the BTO-0.08 fibers were composed of small nanoparticles with about 30-60 nm in diameters. Owing to the

decomposition of PVP during calcination, a porous structure was observed in the fibers. This porous structure is conducive to the improvement of photocatalytic performance because it not only provides a high surface area of the catalysts but also offers many open channels, which could help the reactants go through it easily. The nitrogen adsorption-desorption isotherms curves of samples are shown in Fig. S1 and S2 in the supplementary materials. The BET surface area of $Bi_4Ti_3O_{12}/Bi_2Ti_2O_7$, BTO-0.02, BTO-0.04 and BTO-0.08 are 6.681 m^2/g, 15.102 m^2/g, 16.263 m^2/g and 15.386 m^2/g respectively. Fig. 1f displays high resolution TEM images and fast Fourier transform (FFT) images corresponding to the different area. The HRTEM image reveals that two independent crystal lattices $Bi_4Ti_3O_{12}$ and $Bi_2Ti_2O_7$ were common existence. The lattice fringes observed correspond to the interplanar distances of 0.29 nm and 0.31 nm, which can be assigned to the lattice spacing of $Bi_4Ti_3O_{12}$ (1 7 1) planes and $Bi_2Ti_2O_7$ (6 2 2) planes, respectively.

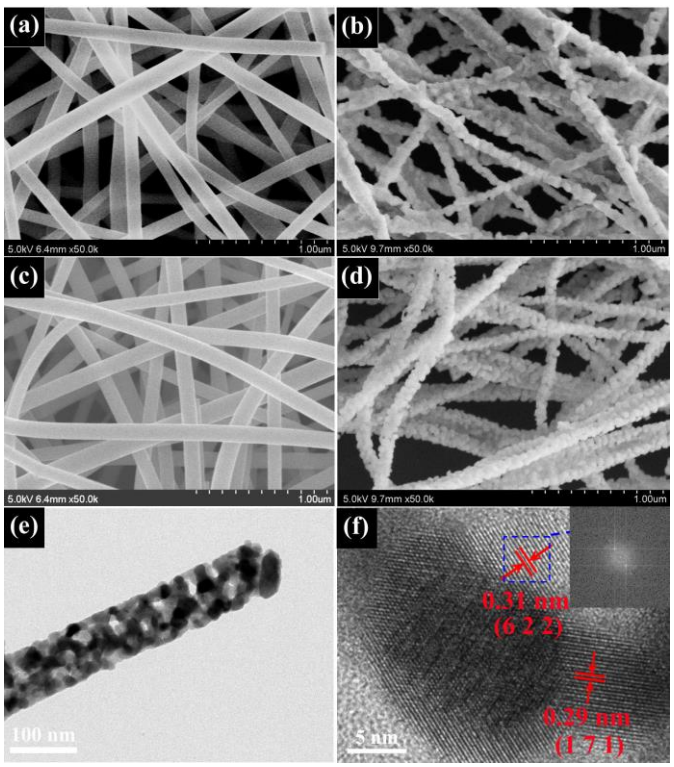

Fig. 1 SEM images of $Bi_4Ti_3O_{12}/Bi_2Ti_2O_7$ fibers (a) before calcination and (b) after calcination; (c) BTO-0.08 fibers before calcination and (d) after calcinations; TEM (e) and HRTEM (f) images for the BTO-0.08 sample, the inset in (f) is a corresponding FFT pattern.

The optical properties of $Bi_4Ti_3O_{12}/Bi_2Ti_2O_7$ fibers and BTO fibers were measured by the UV-visible diffuse reflectance spectra in the range of 200-900 nm. As it could be seen from the curves, the $Bi_4Ti_3O_{12}/Bi_2Ti_2O_7$ fibers exhibit an obvious spectra absorption onset at 400 nm, which is consistent with the band gap absorption edge of $Bi_4Ti_3O_{12}$. It shows little absorbance in the visible-light range. In contrast, the absorbance of the BTO fibers in the visible-light has been improved. As shown in Fig. 2, additional absorption bands ranged from 400 nm to about 800 nm have been observed. The absorbance intensity gradually increases with the increase of Cr dopant amount. And the band gap of BTO samples were also narrowed from 3.1 eV to 2.4 eV gradually, as shown in Fig. S3.

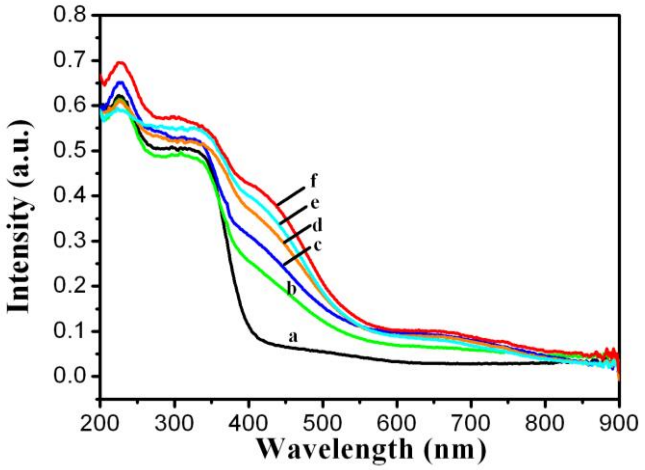

Fig. 2 UV-vis diffuse reflectance spectra of the $Bi_4Ti_3O_{12}/Bi_2Ti_2O_7$ fibers and BTO fibers with different Cr contents. $Bi_4Ti_3O_{12}/Bi_2Ti_2O_7$ (a), BTO-0.01 (b), BTO-0.02 (c), BTO-0.04 (d), BTO-0.06 (e) and BTO-0.08 (f).

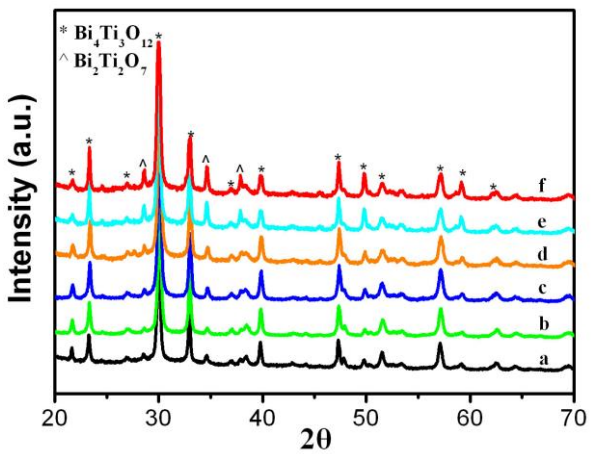

Fig. 3 XRD patterns of the $Bi_4Ti_3O_{12}/Bi_2Ti_2O_7$ fibers and BTO fibers with different Cr contents. $Bi_4Ti_3O_{12}/Bi_2Ti_2O_7$ (a), BTO-0.01 (b), BTO-0.02 (c), BTO-0.04 (d), BTO-0.06 (e) and BTO-0.08 (f).

Fig. 3 shows the X-ray diffraction (XRD) pattern of the $Bi_4Ti_3O_{12}/Bi_2Ti_2O_7$ fibers and BTO fibers. The main diffraction peaks in $Bi_4Ti_3O_{12}/Bi_2Ti_2O_7$ fibers can be assigned to orthorhombic $Bi_4Ti_3O_{12}$ (JCPDS 35-0795). Obviously, there are also additional small diffraction peaks, which can be attributed to cubic $Bi_2Ti_2O_7$ (JCPDS 32-0118). And with increasing the amount of Cr doping, these small peaks gradually rise up. In the crystal lattice of $Bi_4Ti_3O_{12}$ and $Bi_2Ti_2O_7$, Cr and Ti take the same position. The addition of Cr leads to that the ratio of

Cr+Ti/Bi increases, Therefore, $Bi_2Ti_2O_7$ crystalline phase with higher Ti content could be further formed. As shown in BTO-0.08, the amount of $Bi_2Ti_2O_7$ in the electrospun fibers increased obviously. In a word, with increasing the amount of Cr doping, the heterostructure of $Bi_4Ti_3O_{12}/Bi_2Ti_2O_7$ has been enhanced. If more Cr(III) is added into the precursor, only Cr doped $Bi_2Ti_2O_7$ is obtained after calcination (Fig. S4-S6).

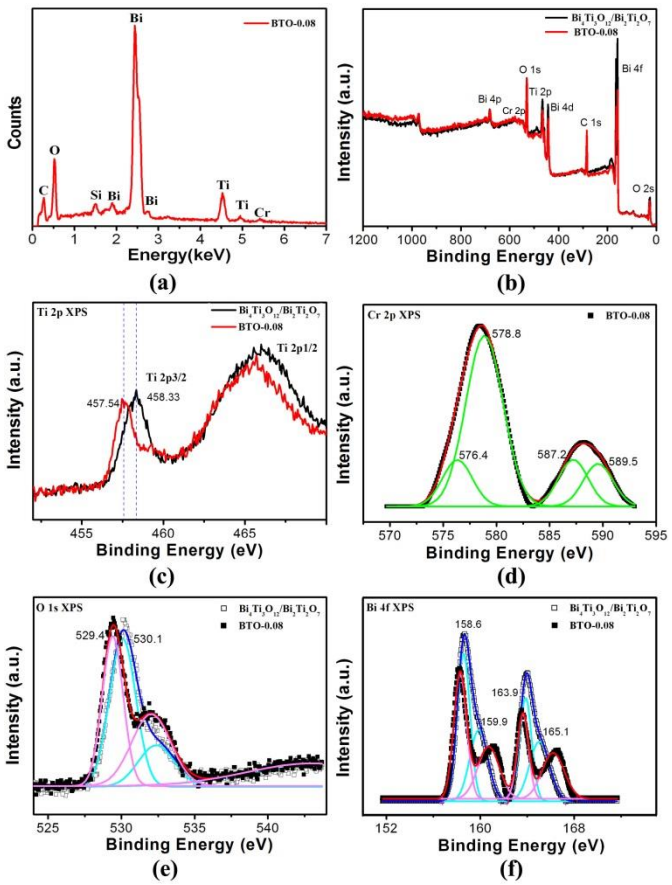

Fig. 4 (a) EDX spectra of BTO-0.08; (b) XPS spectra of $Bi_4Ti_3O_{12}/Bi_2Ti_2O_7$ and BTO-0.08; (c) Ti 2p XPS spectra of $Bi_4Ti_3O_{12}/Bi_2Ti_2O_7$ and BTO-0.08; (d) Cr 2p XPS spectra of BTO-0.08; (e) O 1s XPS spectra of $Bi_4Ti_3O_{12}/Bi_2Ti_2O_7$ and BTO-0.08; (f) Bi 4f XPS spectra of $Bi_4Ti_3O_{12}/Bi_2Ti_2O_7$ and BTO-0.08.

In order to investigate the composition and chemical state of the chromium-doped $Bi_4Ti_3O_{12}/Bi_2Ti_2O_7$, the energy dispersive X-ray analysis (EDX) and X-ray photoelectron spectra (XPS) of $Bi_4Ti_3O_{12}/Bi_2Ti_2O_7$ fibers and BTO-0.08 have been measured. Fig. 4a clearly exhibits signal of Ti, Bi, O and Cr elements in EDX pattern of BTO-0.08, indicated that Cr have doped into $Bi_4Ti_3O_{12}/Bi_2Ti_2O_7$ fibers successfully. This can be further confirmed by the result of XPS. As shown in Fig. 4b, in BTO-0.08 the XPS signals originating from Cr 2p, O 1s, Ti 2p, C 1s and Bi 4f can be identified easily by the binding energies at 578 eV, 531 eV, 465 eV, 284 eV and 169 eV, respectively. Both EDX and XPS results confirm that chromium-doped bismuth titanate fibers form through this simple electrospinning and sintering process. Fig. 4c shows the Ti 2p XPS of $Bi_4Ti_3O_{12}/Bi_2Ti_2O_7$ and BTO-0.08. Clearly, the high resolution Ti 2p XPS spectra of BTO-0.08 have an obvious shift towards low binding energy compared to that of $Bi_4Ti_3O_{12}/Bi_2Ti_2O_7$. As it is seen form the O 1s and Bi 4f XPS spectra, some similar shifts were also observed, which might be caused by the presence of Cr doped. Fig. 4d and S7 show the Cr 2p XPS spectra of BTO-0.08. The two peaks of Cr $2p_{3/2}$ and Cr $2p_{1/2}$ can be split into Cr (III) and Cr (VI) at 576.4 eV, 587.2 eV (Cr(III)) and 578.8 eV, 589.5 eV (Cr(VI)), respectively.[39] The O 1s spectra of $Bi_4Ti_3O_{12}/Bi_2Ti_2O_7$ can be fitted into two Gaussian peaks at 530.1 eV and 532.4 eV, which can be assigned to Bi-O and Ti-O bonds, respectively.[30] And as shown in Fig. 4e, after Cr doped, the peak corresponding to Ti-O bonds shows an increase. This result was consistent with the result of XRD. With the increase contents of Cr, the $Bi_2Ti_2O_7$ phase which contains more Ti-O bonds increased gradually. The Bi 4f XPS spectra further confirm the fact. As shown in Fig. 4f, two new shoulders at around 161.0 eV and 166.6 eV are observed in BTO-0.08, which can be attributed to the Cr doped $Bi_2Ti_2O_7$. As Cr doped, the peaks of $Bi_2Ti_2O_7$ at 159.9 eV and 165.1 eV were shifted to 160.7 eV and 166.2 eV respectively. Simultaneously, the ratio of peaks at high binding energy ($Bi_2Ti_2O_7$) and at low binding energy ($Bi_4Ti_3O_{12}$) increases, indicating that the amount of $Bi_2Ti_2O_7$ increases with increasing the amount of Cr doping.

Photocatalytic activity, Photocurrent response and Photoluminescence spectra

The photocatalytic degradation of MO under visible-light irradiation ($\lambda > 420$ nm) had been chosen as a model reaction to evaluate the photocatalytic activities of $Bi_4Ti_3O_{12}/Bi_2Ti_2O_7$ and BTO fibers. Fig. 5a shows the time profiles of MO photocatalytic degradation over $Bi_4Ti_3O_{12}/Bi_2Ti_2O_7$ and BTO fibers under visible light irradiation. Because these as-prepared samples are mesoporous materials, an obvious adsorption of MO on the fibers was observed in all case before irradiation. And with the increase contents of Cr in fibers, the adsorption was enhanced, which might be related to the larger surface area and surface charge changes of BTO. In the case of BTO-0.08, over 50% MO molecules have been absorbed on the surface of BTO-0.08 fibers after stirred in the dark for 30 min. Under the visible light irradiation, there was negligible self-photodegradation of MO. For $Bi_4Ti_3O_{12}/Bi_2Ti_2O_7$, only 4.8% of MO was degraded after irradiated under visible light for 5 h, because of its lower visible light adsorption. The photocatalytic performances of BTO fibers were influenced by the contents of Cr doping. With the increase amount of Cr, the photocatalytic activity of the BTO fibers was enhanced. As shown in Fig. 5a, the degradation efficiency of MO by BTO-0.01 (b), BTO-0.02 (c) and BTO-0.04 (d) was about 18.9%, 39.4% and 61.9% respectively irradiated under visible light for 5 h. For BTO-0.06 (e) and BTO-0.08 (f) (Fig. S8), the MO molecules were almost degraded completely (the efficiency reach 98%) after visible light irradiation for 150 min and 90 min respectively. Although the degradation efficiency might be influenced by the initial adsorption, the kinetic linear simulation curves of MO photodegradation can directly reveal the photocatalytic activity

of these BTO fibers. As shown in Fig. S9, using the initial concentration of the MO after adsorption–desorption equilibrium as C_0, the calculated curves of k for the degradation using $Bi_4Ti_3O_{12}/Bi_2Ti_2O_7$, BTO-0.01, BTO-0.02, BTO-0.04, BTO-0.06 and BTO-0.08 as catalyst are 1.73634×10^{-4}, 8.8116×10^{-4}, 0.00206, 0.00494, 0.023 and 0.03745 min^{-1}, respectively. Clearly, BTO-0.08 possesses the highest photocatalytic activity under visible light irradiation, owing to its enhanced visible light response. Fig. S10 shows the cycling runs using BTO-0.08 as catalyst for photodegradation of MO under visible light irradiation. With the process of recycle, the initial concentration of the MO after adsorption–desorption equilibrium was increased gradually, which might be influenced by the absorbed MO molecules on the BTO fibers. Recycled BTO fibers have lower absorbance capability than initial blank BTO fibers, because of the loss of sample recycling and the surface charge changes of BTO fibers. However, the photodegradation efficiency of three runs was all about 50% after visible light irradiation for 90 min. That means BTO-0.08 have a good stability.

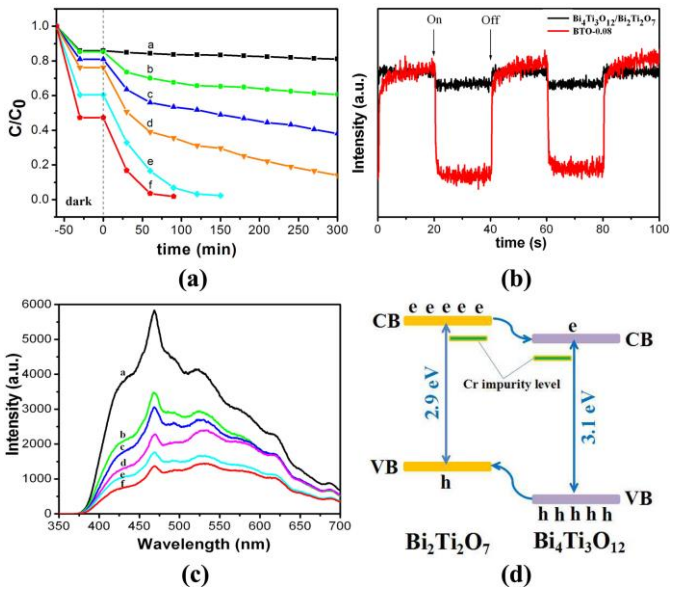

Fig. 5 (a) Degradation profiles of MO, using $Bi_4Ti_3O_{12}/Bi_2Ti_2O_7$ (a), BTO-0.01 (b), BTO-0.02 (c), BTO-0.04 (d), BTO-0.06 (e) and BTO-0.08 (f) as photocatalyst, where C is the concentration of the MO, C_0 is the initial concentration of MO; (b) Transient photocurrent response of $Bi_4Ti_3O_{12}/Bi_2Ti_2O_7$ and BTO-0.08 in 0.5 M Na_2SO_4 aqueous solutions under visible-light irradiation at 0 V *vs.* Hg/Hg_2Cl_2; (c) The PL spectra for $Bi_4Ti_3O_{12}/Bi_2Ti_2O_7$ (a), BTO-0.01 (b), BTO-0.02 (c), BTO-0.04 (d), BTO-0.06 (e) and BTO-0.08 (f), respectively; (d) Schematic representation of band edges of Cr-doped $Bi_4Ti_3O_{12}/Bi_2Ti_2O_7$.

In order to verify the enhanced visible light photocatalytic activity and the improvement in charge separation of BTO fibers, the transient photocurrent responses and the photoluminescence (PL) emission spectra of $Bi_4Ti_3O_{12}/Bi_2Ti_2O_7$ and BTO-0.08 were measured. As shown in Fig. 5b, both $Bi_4Ti_3O_{12}/Bi_2Ti_2O_7$ and BTO-0.08 fibers have an enhanced reproducible photocurrent response under visible light irradiation, when the light was switched on and off. The photocurrent density of BTO-0.08, 6.053×10^{-5} mA/cm^2, was 8 times higher than that of $Bi_4Ti_3O_{12}/Bi_2Ti_2O_7$ (7.47×10^{-6} mA/cm^2), implying that the visible light photocatalytic activity and the charge separation of BTO-0.08 was significantly enhanced (Fig. S11 and S12). This can be attributed to the improvement of visible light adsorption and the enhanced heterojunction structures as Cr doped. Fig. 5c shows the PL spectra of $Bi_4Ti_3O_{12}/Bi_2Ti_2O_7$, BTO-0.02 and BTO-0.08 fibers. With an excitation wavelength at 320 nm, the emission intensity of BTO-0.02 and BTO-0.08 fibers was reduced clearly compared with that of $Bi_4Ti_3O_{12}/Bi_2Ti_2O_7$. The BTO-0.08 has the largest decrease in the intensity of the PL peaks. These results reveal that the recombination of photogenerated charge carriers can be effectively inhibited as Cr doped. Fig. 5d shows the possible schematic representation of the band edges of Cr-doped $Bi_4Ti_3O_{12}/Bi_2Ti_2O_7$. As a result of XRD and XPS, when Cr was added in the fibers, some of Ti centers could be substituted by Cr, which make the increase amount of Ti/Bi, thus resulting in the further formation of $Bi_2Ti_2O_7$. With the increase contents of $Bi_2Ti_2O_7$, the type II heterojunction structure of $Bi_4Ti_3O_{12}/Bi_2Ti_2O_7$ was enhanced. The recombination of photogenerated charge carriers was effectively inhibited. Furthermore, $Bi_2Ti_2O_7$ possess the band gap of 2.9 eV,[40] which can improve the light adsorption of $Bi_4Ti_3O_{12}$. On the other hand, as Cr doped, the spectra response of $Bi_4Ti_3O_{12}$ and $Bi_2Ti_2O_7$ could also be further extended. Therefore, the Cr-doped $Bi_4Ti_3O_{12}/Bi_2Ti_2O_7$ fibers show a good photocatalytic performance.

Conclusions

In summary, we have fabricated a series of Cr-doped $Bi_4Ti_3O_{12}/Bi_2Ti_2O_7$ heterostructures fibers by one-step of facile and economical electrospinning/calcination route. SEM and TEM reveal that the diameters of the as-prepared fibers are about 100 ±30 nm in size. And with the increase contents of Cr, the light adsorption of $Bi_4Ti_3O_{12}$ and $Bi_2Ti_2O_7$ has been improved. And the amount of $Bi_2Ti_2O_7$ in the fibers has been also raised, thus enhanced the type II heterojunction structure of $Bi_4Ti_3O_{12}/Bi_2Ti_2O_7$. The photogenerated charge separation of these Cr-doped BTO fibers has been further enhanced. Therefore, photocatalytic tests display that the as-prepared Cr-doped $Bi_4Ti_3O_{12}/Bi_2Ti_2O_7$ fibers exhibit good photocatalytic activity for photodegradation of methyl orange (MO) under visible light irradiation.

Acknowledgements

The authors thank the National Natural Science Foundation of China (No. 21301166, 21201159, and 61176016), Science and Technology Department of Jilin Province (No. 20130522127JH, and 20121801) are gratefully acknowledged. Z. S. thanks the support of the "Hundred Talent Program" of CAS. Supported by open research fund program of State Key Laboratory of Luminescence and Applications (Changchun Institute of Optics, Fine Mechanics and Physics, CAS) and Key Laboratory of

Functional Inorganic Material Chemistry (Heilongjiang University), Ministry of Education, P. R. China.

Notes and references

[a] State Key Laboratory of Luminescence and Applications, Changchun Institute of Optics, Fine Mechanics and Physics, Chinese Academy of Sciences, 3888 East Nanhu Road, Changchun 130033, People's Republic of China. Email: sunzc@ciomp.ac.cn

[b] Key Laboratory of Polyoxometalate Science of Ministry of Education, Department of Chemistry, Northeast Normal University, Ren Min Street No. 5268, Changchun, Jilin, 130024, People's Republic of China. wangeb889@nenu.edu.cn

[c] State Key Laboratory of Applied Optics, Changchun Institute of Optics, Fine Mechanics and Physics, Chinese Academy of Sciences, Changchun 130033, China.

Electronic Supplementary Information (ESI) available: BET, XRD, UV-Vis, XPS, Transient photocurrent response, EIS . See DOI: 10.1039/b000000x/

1 M. R. Hoffmann, S. T. Martin, W. Choi and D. W. Bahnemann, *Chem. Rev.*1995**, 95**, 69-96.
2. J. Lasek, Y. Yu and J. C.S. Wu, *J. Photochem. Photobiol C Photochem Rev*. 2013, **14**, 29-52.
3. C. Chen, W. Ma and J. Zhao, *Chem. Soc. Rev*. 2010, **39**, 4206-4219.
4. H. Wang, L. Zhang, Z. Chen, J. Hu, S. Li, Z. Wang, J. Liu and X. Wang, *Chem. Soc. Rev*. 2014, **43**, 5234-5244.
5. X. Chen, S. Shen, L. Guo and S. S. Mao, *Chem. Rev*. 2010, **110**, 6503-6570.
6. Q. Li, B. Guo, J. Yu, J. Ran, B. Zhang, H. Yan and J. R. Gong, *J. Am. Chem. Soc*. 2011, **133**, 10878-10884.
7. Q. Xiang, J. Yu and M. Jaroniec, *J. Am. Chem. Soc*. 2012, **134**, 6575-6578.
7. M. Marszewski, S. Cao, J. Yu and M. Jaroniec, *Mater. Horiz.* 2015, DOI: 10.1039/C4MH00176A.
8. J. Yu, J. Low, W. Xiao, P. Zhou and M. Jaroniec, *J. Am. Chem. Soc.* 2014, **136**, 8839-8842.
9. W. Ong, L. Tan, S. Chai and S. Yong, *Chem. Commun.* 2015, **51**, 858-861.
10. X. Li, J. Yu, J. Low, Y. Fang, J. Xiao and X. Chen, *J. Mater. Chem. A.* 2015, **3**. 2485-2534.
11. H. Cheng, B. Huang and Y. Dai, *Nanoscale.* 2014, **6**, 2009-2026.
12. R. Li, H. Han, F. Zhang, D. Wang and C. Li, *Energy Environ. Sci.* 2014, **7**, 1369-1376.
13. J. Tian, Y. Sang, G. Yu, H. Jiang, X. Mu and H. Liu, *Adv. Mater.* 2013, **25**, 5075-5080.
14. H. Li, J. Liu, W. Hou, N. Du, R. Zhang and X. Tao, *Appl. Catal. B: Environ.* 2014, **160**, 89-97.
15. Z. Zhao, J. Tian, D. Wang, X. Kang, Y. Sang, H. Liu, J. Wang, S. Chen, R. I. Boughton and H. Jiang, *J. Mater. Chem.* 2012, **22**, 23395-23403.
16. X. Gao, H. B. Wu, L. Zheng, Y. Zhong, Y. Hu and X. W. Lou, *Angew. Chem. Int. Ed.* 2014, **53**, 5917-5921.
17. Y. Liu, M. Zhang, L. Li and X. Zhang, *Appl. Catal. B: Environ.* 2014, 160, 757-766.
18. R. He, S. Cao, P. Zhou and J. Yu, Chinese J Ctatal. 2014, 35, 989-1007.
19. Y. Li, L. Dang, L. Han, P. Li, J. Wang and Z. Li, *J. Mol. Catal A: Chem.* 2013, **379**, 146-151.
20. P. Hao, Z. Zhao, J. Tian, Y. Sang, G. Yu, H. Liu, S. Chen and W. Zhou, Acta Materialla. 2014, 62, 258-266.
21. J. Hou, R. Cao, S. Jiao, H. Zhu and R. V. Kumar, *Appl. Catatl B: Environ.* 2011, **104**, 399-406.
22. J. Hou, S. Jiao, H. Zhu and R. V. Kumar, *J. Solid. State. Chem.* 2011, **184**, 154-158.
23. W. Zhao, Z. Jia, E. Lei, L. Wang, Z. Li and Y. Dai, *J. Phys. Chem. Solids.* 2013, **74**, 1604-1607.
24. W. F. Yao, X. H. Xu, H. Wang, J. T. Zhou, X. N. Yang, Y. Zhang, S. X. Shang and B. B. Huang, *Appl. Catal B: Environ.* 2004, **52**, 109-116.
25. A. Kudo and S. Hijii, *Chem. Lett.* 1999, **28**, 1103-1104.
26. X. Lin, P. Lv, Q. Guan, H. Li, H. Zhai and C. Liu, *Appl. Surf. Sci.* 2012, **258**, 7146-7153.
27. P. S. Kumar, J. Sundaramurthy, S. Sundarrajan, V. J. Babu, G. Singh, S. I. Allakhverdiev and S. Ramakrishna, *Energy. Environ. Sci.* 2014, **7**, 3192-3222.
28. C-L. Zhang and S-H. Yu, *Chem. Soc. Rev.* 2014, **43**, 4423-4448.
29. D. Hou, W. Luo, Y. Huang, J. C. Yu and X. Hu, *Nanoscale*. 2013, **5**, 2028.
30. D. Hou, X. Hu, P. Hu, W. Zhang, M. Zhang and Y. Huang, *Nanoscale*. 2013, **5**, 9764-9772.
31. X. Lin, Q. Guan, Y. Zhang, T. Liu, C. Zou, C. Liu and H. Zhai, J. Phys. Chem. Solids. 2013, 74, 1254-1262.
32. W. F. Yao, H. Wang, X. H. Xu, X. N. Yang, Y. Zhang, S. X. Shang and M. Zhang, *Appl. Catal A: General.* 2003, **251**, 235-239.
33. J. Hou, R. Cao, Z. Wang, S. Jiao and H. Zhu, J. Mater. Chem. 2011, 21, 7296-7301.
34. W. Zhao, Y. Jin, C. H. Gao, W. Gu, Z. M. Jin, Y.L. Lei and L. S. Liao, *Mater. Chem Phys.* 2014, **143**, 952-962.
35. K. Chen, R. Hu, X. Feng, K. Xie, Y. Li and H. Gu, *Ceramics International.* 2013, **39**, 9109-9114.
36. X. B. Meng, J. Miao, Y. Zhao, S. Z. Wu, X. G. Xu, S. G. Wang and Y. Jiang, *J Mater Sci: Mater Electron.* 2014, **25**, 1423-1428.
37. G. Liu, L.-C. Yin, J. Wang, P. Niu, C. Zhen, Y. Xie, and H.-M. Cheng, *Energy Environ. Sci.* 2012, **5**, 9603-9610.
38. H. Yu, Y. Zhao, C. Zhou, L. Shang, Y. Peng, Y. Cao, L.-Z. Wu, C.-H. Tung and T. Zhang, *J. Mater. Chem. A.* 2014, **2**, 3344-3351.
39. K. M. Parida, A. Nashim and S. K. Mahanta, *Dalton Trans.* 2011, **40**, 12839-12845.
40. W. Wei, Y. Dai and B. Huang, *J. Phys. Chem. C.* 2009, **113**, 5658-5663.

TOC Figure

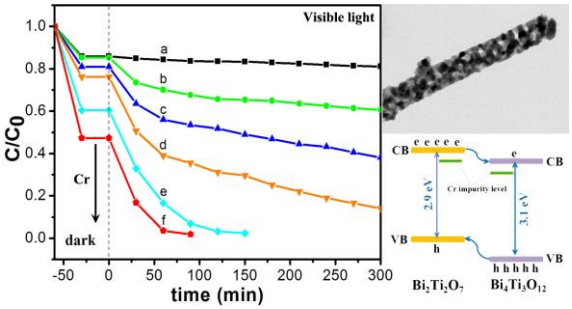

Cr-doped $Bi_4Ti_3O_{12}/Bi_2Ti_2O_7$ nanofibers have been synthesized by electrospinning/calcination route, which shows good visible-light activity for photodegradation of methyl orange.